CO Oxidation on $Rh/SiO_2/Mo(112)$ Model Catalysts at Elevated Pressures

Sean M. McClure, M. Lundwall, F. Yang, Z. Zhou, and D. W. Goodman*

Department of Chemistry, Texas A&M University, P.O. Box 30012, College Station, Texas 77842-3012

Received: October 9, 2008; Revised Manuscript Received: April 6, 2009

Well-defined model catalyst samples, prepared under ultra-high-vacuum (UHV) conditions, hold the potential of bridging the gap between traditional surface science and technical catalysis studies. However, work remains to understand and characterize reaction kinetics of such samples under more realistic pressure conditions, specifically, how reaction kinetics of a well-studied reaction (such as CO oxidation) over model surfaces compares to single-crystal surfaces studied under identical conditions. Here, the CO oxidation reaction under elevated-pressure conditions ($P = 8.0$ Torr) and CO-rich reaction conditions is used as a probe reaction to characterize Rh/SiO_2 model catalyst samples, prepared on a Mo(112) substrate under UHV conditions, in a contiguous high-pressure reactor cell-UHV surface analysis chamber. CO oxidation reaction kinetics are studied as a function of O_2/CO partial pressures (from 1/1 to 1/10 O_2/CO) and Rh coverage ($\theta_{Rh} = 0.25-10$ ML), along with measurements on a Rh(111) single crystal for direct comparison. CO desorption measurements on the Rh/SiO_2 films and STM measurements of Rh particles on ultrathin SiO_2 films at $T = 300$ K have been obtained at various Rh coverages to provide two additional methods to estimate reactive sites. Results demonstrate that, under the reaction conditions employed, CO oxidation reaction on $Rh/SiO_2/Mo(112)$ exhibits O_2/CO dependencies and reaction activation energies similar to those observed on single-crystal samples. These data show that model catalyst samples can be used to gain qualitative and quantitative reactivity data over a range of elevated-pressure reaction conditions. Measurements of CO oxidation under CO-rich conditions can provide a reasonable estimate of the number of active sites on Rh model catalyst surfaces, thus providing a useful starting point for future studies of particle- and structure-dependent reactions on model catalyst surfaces.

Introduction

Technical catalyst surfaces employed in practical systems are typically composed of an active metal phase dispersed on a metal oxide support. Fundamental studies of catalytic reactions on these surfaces are complicated by such factors as mass transfer issues, distribution of particle sizes, and convolution of support effects. Additionally, technical catalyst surfaces are not amenable to many "traditional" surface spectroscopies, making fundamental studies difficult to conduct on working catalyst surfaces. Thus, researchers have often focused on well-defined, metal single crystals as a simplified model system for fundamental insights into the kinetics of catalytic reactions, such as CO oxidation reaction at elevated pressures,[1−3] to compare with complementary technical catalyst studies.[3−7] Though much progress and understanding has been made employing single-crystal surfaces, these surfaces do not allow study of variables, such as support effects and particle size effects, factors that can affect the activity and selectivity of surface-catalyzed reactions. Bridging this material gap between traditional surface science and technical catalyst studies has been an active and challenging area of research in catalysis.

Recently, progress and research in surface science techniques have allowed for investigations of more realistic and complex model catalyst samples prepared and characterized in the UHV environment—oxide-supported metal particles that aim to better mimic the active surfaces of working catalysts.[8,62−64] Recipes developed by several groups have demonstrated the ability to prepare an assortment of metal oxide films (such as SiO_2[9−12]) on single-crystal substrates under UHV conditions. These films, coupled with vapor deposition of metal particles, allow for the creation of planar model surfaces for use in investigations of supported metal particles, surfaces that are amenable to traditional surface science spectroscopies. These surfaces enable fundamental investigations of variables, such as support effects, particle size/morphology effects, and particle sintering behavior, which can exert influence on the kinetics of catalytic reactions on supported catalysts.

Due to its fundamental and practical importance, metal-oxide-supported Rh model catalyst samples have been prepared and characterized by a number of groups using a variety of synthetic techniques. Insights into particle morphology, particle sintering, interaction with CO and O_2 ambients, and low-pressure CO oxidation kinetics have been acquired for a variety of oxide-supported Rh systems (alumina,[13−19] silica,[20−22] titania,[23−26] and magnesium oxide[15,19,27] single-crystal and thin-film substrates). Additionally, recent solution-based methods for generating monodispersed Rh nanocubes supported on Si have allowed for ex situ CO oxidation kinetic measurements on well-defined Rh particles.[28] Several recent studies employing such surfaces have been utilized to investigate Rh and Rh bimetallic particles at elevated pressures via ambient-pressure spectroscopic techniques.[53,54]

With regards to CO oxidation reaction kinetics, much work still remains to fully investigate the behavior of this fundamental reaction on Rh model catalyst systems. While reactivity on Rh surfaces at elevated pressures under high O_2/CO conditions remains a currently debated topic,[35,36,55] CO oxidation under CO-rich conditions (low O_2/CO ratios) exhibits structure-insensitive reaction kinetics.[1−6,37] As such, CO oxidation kinetic measure-

* Corresponding author. Phone: +1 979 845 0214. Fax: +1 979 845 6822. E-mail: goodman@mail.chem.tamu.edu.

10.1021/jp808953v CCC: $40.75
Published on Web 05/07/2009

ments under these conditions could potentially be employed as a probe reaction to directly compare model catalyst and single-crystal samples under identical reaction conditions and experimental setup and, thus, to investigate the qualitative and quantitative agreement regarding reaction rates, activation energies, and number of active Rh sites.

In this study, we employ CO oxidation as a probe reaction to characterize Rh/SiO_2/Mo(112) model catalyst samples and their relationship to single-crystal surfaces. Our primary aim in this study is to develop an understanding of the extent of qualitative and quantitative agreement between CO oxidation kinetic data obtained on Rh/SiO_2 model catalyst samples and Rh single-crystal samples under elevated-pressure conditions ($P = 8.0$ Torr). Model catalyst results are compared with data collected on a Rh(111) single-crystal sample to assess kinetic behavior and O_2/CO dependence of the CO oxidation reaction on the model catalyst surfaces. To the best of our knowledge, this is the first attempt to directly compare elevated-pressure CO oxidation reaction kinetics on Rh model catalyst surfaces to Rh single-crystal surfaces (prepared entirely in situ in UHV) under identical reaction and reactor conditions. For additional characterization, CO desorption measurements on Rh/SiO_2 samples have been obtained, and STM data (in a separate STM system) have been collected for Rh deposited on ultrathin SiO_2 films (1 ML, 3 Å) to provide estimates of particle size and number of active Rh sites as a function of Rh coverage. Taken together, the results demonstrate that Rh/SiO_2 model catalysts can be effectively employed to gain both quantitative and qualitative insights into reaction kinetics at elevated pressures. Furthermore, the CO oxidation reaction under CO-rich reaction conditions provides a useful method for estimating active sites present on model catalyst surfaces. These understandings will be important in current and ongoing work investigating more complicated, structure-sensitive reactions on such model catalyst surfaces.

Experimental Section

Experiments were conducted in a coupled high-pressure reactor-UHV surface analysis chamber described previously, which allows for in situ translation of surfaces prepared in the UHV chamber into the reactor cell.[29] A similar setup has been employed successfully in a number of recent elevated-pressure kinetic studies of CO oxidation over Pt-group single crystals.[37−39] A Mo(112) single-crystal sample (circular disk, 0.986 cm diameter) was used as a substrate for film growth. The sample is resistively heated through a Ta wire lead welded to the edge of the sample, with temperature control and measurement accomplished via a W/Re thermocouple spot welded to the rear of the sample. Rh(111) reactivity measurements were conducted on a Rh(111) single-crystal sample (circular disk, 0.963 cm diameter). Mo(112) and Rh(111) sample cleanliness was achieved with Ar^+ sputtering and annealing cycles and assessed via Auger electron spectroscopy (AES).

Model catalyst surfaces were generated in two steps: (1) preparation of SiO_2 film on the Mo(112) substrate and (2) vapor deposition of Rh metal on the SiO_2/Mo(112) sample. Several laboratories[9−12] have developed procedures for preparation of ultrathin (1 ML) and thicker (several monolayers) SiO_2 films; a vapor deposition recipe similar to that developed previously in our laboratory was utilized for SiO_2 film growth.[12] Si dosing was accomplished by vapor deposition from a home-built doser consisting of Si held by a Ta filament. Silica films were grown by alternating steps of (1) Si dosing at a sample temperature of $T = 650$ K in $P \sim 5 \times 10^{-6}$ Torr O_2, followed by (2) annealing at $T = 800$ K in $P \sim 1 \times 10^{-5}$ Torr O_2. This procedure was performed on both sides of the sample such that *both* faces of the Mo(112) were covered with a SiO_2 film. After Si dosing was completed, the sample was annealed at $T = 1000$ K for 20 min in $P \sim 2 \times 10^{-5}$ Torr O_2 ambient to complete oxidation of the SiO_2 film. AES spectra of the SiO_2 film are similar to those previously observed,[9,12] indicating a fully oxidized Si (in SiO_2) AES feature (78 eV) with a SiO_2 film thickness that almost completely attenuated the Mo (187 eV) AES feature (this corresponds to a 5 ML (15 Å) SiO_2 film[9]).

Rh particles are generated on the SiO_2 film by Rh vapor deposition (at a sample temperature of $T = 300$ K), using a home-built evaporative doser (high-purity Rh wire heated on a tungsten filament). Rh was dosed *only* on the front side of the SiO_2/Mo(112) sample. Rh dosing rate on the SiO_2 was calibrated with a breakpoint analysis of the primary Rh AES feature (302 eV) on the Mo(112) surface. This analysis showed a breakpoint at a Rh(302 eV)/Mo(187 eV) AES ratio of ~0.5. For the purposes of dose calibration, this ratio will be referred to herein as a monolayer equivalent coverage of Rh; typical Rh deposition rates were ~0.25 ML/min. To assess the uniformity of the deposited Rh coverage across the sample, AES measurements were conducted at various points across the sample surface for a Rh/Mo(112) coverage of $\theta_{Rh} = 1$ ML. On the basis of these measurements, we estimate that the Rh coverage across the sample varies no more than ±15% from the stated coverage.

CO oxidation reactions were conducted in a batch reactor mode in the contiguous high-pressure cell ($V_{reactor} = 0.3$ L). O_2/CO mixtures were premixed (prior to charging reaction cell) with ultra-high-purity O_2 and CO; CO was further purified through a heated molecular sieve and subsequent LN_2 cryogenic trap to remove any carbonyl impurities; O_2 was used without further purification. For example, a $P = 8.0$ Torr charge of a (1/1) O_2/CO reaction mixture contains $P_{O_2} = 4.0$ Torr and $P_{CO} = 4.0$ Torr. Initial reaction rates (<10% conversion) were measured with a baratron gauge in a technique described previously.[30] Control reactivity experiments conducted on prepared SiO_2 films (without Rh) to estimate any background contributions to the reaction measurements demonstrated that background reaction rates were typically no more than a few percent of the overall reaction rate at a given temperature. This indicates that essentially all CO_2 production arises from the presence of the Rh particles.

In addition to reactivity measurements, two other methods were employed to assess the number of active sites present on Rh/SiO_2 samples as a function of Rh coverage. CO temperature-programmed desorption (TPD) experiments were conducted to provide an additional estimate of the number of Rh surface sites from CO chemisorption on particle samples compared to Rh(111) single crystals. For these experiments, Rh metal is deposited on the SiO_2 film and the sample is then run through an initial TPD cycle in vacuo. Next, a saturation coverage of 4 L CO is dosed on the sample at $T_{ads} = 175$ K. The sample was then heated at a rate of $\beta \sim 5$ K/s from $T = 130-700$ K to obtain CO thermal desorption spectra. TPD spectra are obtained with negligible line of sight to the quadrupole from the sample. Reference TPD spectra were obtained on the Rh(111) single-crystal sample for a saturation 4 L CO coverage. Since the number of Rh surface atoms ($N_{Rh(111)}$) can be estimated on the Rh(111) single crystal, the integrated TPD spectra from the Rh(111) single crystal ($A_{TPD,Rh(111)}$) can be used to convert particle TPD spectra integrated area ($A_{TPD,particles}$) into an estimate of the number of Rh sites (N_{Rh/SiO_2})on Rh/SiO_2/Mo(112) samples for a desired Rh coverage: ($A_{TPD,particles}$/

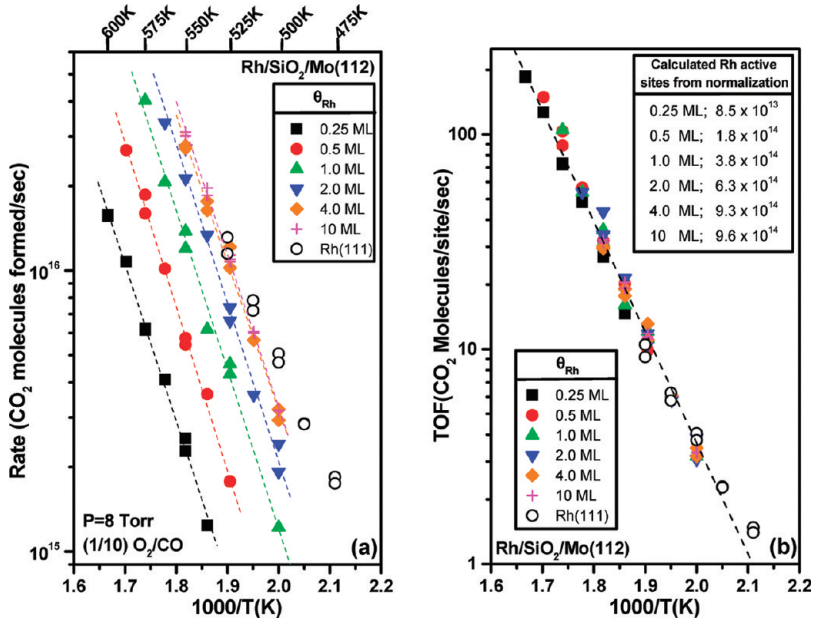

Figure 1. (a) CO_2 reaction rate data, CO_2 molecules formed/s vs 1000/T (K), for various Rh coverages (θ_{Rh}) on Rh/SiO_2/Mo(112) model catalyst samples: (□) 0.25 ML, (●) 0.5 ML, (▲) 1.0 ML, (▼) 2.0 ML, (♦) 4.0 ML, (+) 10 ML. CO_2 reaction rate data obtained over Rh(111) (○), conducted under the same reaction conditions. Typical error in reactivity measurements, based on replicate measurements, is ±10%. (b) CO_2 reaction rate data, from Figure 1a, normalized to Rh(111) data to obtain reaction rate in terms of TOF [CO_2 molecules formed/(site s)]: (□) 0.25 ML, (●) 0.5 ML, (▲) 1.0 ML, (▼) 2.0 ML, (♦) 4.0 ML, (+) 10 ML, (○) Rh(111). Each set of Rh coverage reaction data was linear best fit to the Rh(111) reaction data. The calculated activation energy obtained from normalization of all the Rh particle and Rh(111) single-crystal data (dotted line) is E_a = 100 ± 3 kJ/mol. Typical error in reactivity measurements, based on replicate measurements, is ±10%.

$A_{TPD,Rh(111)})N_{Rh(111)} = N_{Rh/SiO_2}$. These estimates are then put into terms of Rh sites/cm^2 by dividing by the Mo(112) sample area.

STM measurements were conducted in a separate vacuum system. Rh particles were deposited on an ultrathin (1 ML SiO_2) film at T = 300 K under UHV conditions. The ultrathin silica film was prepared by the oxidization of deposited Si atoms on Mo(112) and subsequent annealing to remove multilayer SiO_2. Prior to Si deposition, the sample was flashed to 2100 K and then oxidized in 5 × 10^{-8} Torr O_2 at 850 K for 7 min. A p(2 × 3)−O surface was obtained after the oxidation. The silica film was then prepared by depositing less than 1 ML of Si onto a Mo(112)-p(2 × 3)−O surface, followed by annealing at 800 K in 5 × 10^{-8} Torr O_2 for 5 min, then increasing the temperature to 1200 K for an additional 10 min. This Si deposition/oxidation/annealing procedure was repeated several times until a constant Si/Mo AES ratio was achieved. The silica film was then annealed in UHV at 1200 K for 5 min.

Results

Rh Coverage Dependent Reactivity Measurements. Shown in Figure 1a are reactivity measurements [molecules CO_2 formed/s vs 1000/T (K)] obtained from a series of Rh/SiO_2 model catalyst samples with varying Rh coverage (θ_{Rh} = 0.25−10 ML) using a (1/10) O_2/CO gas mixture along with data obtained from the Rh(111) single crystal. As the data illustrate, increasing Rh coverages results in an increased rate of CO_2 formation as expected. Temperature dependence shows Arrhenius behavior for the temperatures and coverages studied, exhibiting an activation energy of E_a = 100−110 kJ/mol for all coverages studied. This value is in good agreement with the consensus of literature values (E_a = 100−120 kJ/mol) obtained on Rh single crystals and technical catalysts.[1−5] Experiments conducted with the (1/10) O_2/CO mixture under the conditions shown in the figure demonstrated repeatable behavior (i.e., samples could be run repeatably throughout the temperature ranges with negligible changes to the measured reaction rate). Replicate measurements displayed for several of the conditions in the figure demonstrate the repeatability of the measured reaction rate upon repeated reaction. This observation suggests that, for the CO-rich conditions [(1/10) O_2/CO] of Figure 1a, changes in particle reactivity due to reaction are minimal, though it should be noted that changes in particle morphology could occur upon exposure of Rh particles to the reaction mixture prior to reaction. As will be discussed shortly, deactivation occurred with respect to activity as the temperature and or O_2 partial pressure of the gas mixture increased to a critical point (T > 600 K with (1/1) O_2/CO).

Catalytic activity is typically defined in terms of TOF (molecules of CO_2 produced per site per s). CO oxidation on Rh single-crystal and technical catalyst surfaces under similar CO-dominant conditions has been shown to exhibit structure-insensitive kinetics.[1−6,37] Thus, a plot of the Rh/SiO_2/Mo(112) and Rh(111) data of Figure 1a in terms of TOF will be coincident for a structure-insensitive reaction. Thus, the Rh/SiO_2/Mo(112) and Rh(111) reactivity data of Figure 1a can be utilized to obtain an estimate of the number of active sites present on the Rh/SiO_2 as a function of Rh coverage. Since the Rh(111) reactivity data in Figure 1a have been obtained on a single-crystal sample (Rh(111) surface density = 1.6 × 10^{15} atoms/cm^2; single-crystal area = 1.5 cm^2 on front and back), Rh/SiO_2/Mo(112) data can be normalized to the Rh(111) single-crystal data to obtain estimates of the number of active Rh sites. This exercise is visualized in Figure 1b, which is an Arrhenius plot of the data of Figure 1a in terms of TOF, where Rh/SiO_2/Mo(112) reactivity data for the various coverages have been normalized by an appropriate number of sites such that the plots are normalized to the Rh(111) single-crystal data (linear least-squares fit). The number of sites obtained from normalization are shown in the figure for the coverages (θ_{Rh} = 0.25−10 ML).

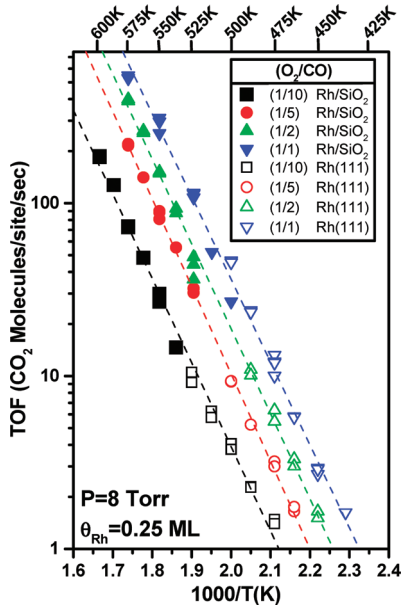

Figure 2. CO_2 reaction rate data {TOF [CO_2 molecules formed/(site s)] vs 1000/T (K)} performed for various O_2/CO gas mixture ratios over a Rh/SiO_2/Mo(112) surface with $\theta_{Rh} = 0.25$ ML Rh coverage: (□) (1/10) O_2/CO, (●) (1/5) O_2/CO, (▲) (1/2) O_2/CO, (▼) (1/1) O_2/CO. Shown as open symbols are corresponding reaction data taken on Rh(111) single-crystal samples: (□) (1/10) O_2/CO, (○) (1/5) O_2/CO, (△) (1/2) O_2/CO, (▽) (1/1) O_2/CO. Particle data are normalized using the estimate of the number of sites obtained for $\theta_{Rh} = 0.25$ ML coverage in Figure 1. Typical error in reactivity measurements, based on replicate measurements, is ±10%.

The calculated activation energy obtained from normalization of all the Rh particle and Rh(111) single-crystal data (dotted line) is $E_a = 100 \pm 3$ kJ/mol. On the basis of repeated measurements on samples with an identical Rh coverage, we estimate that the value obtained by this method has an error of ±20% to the quantitative value reported. As one would expect, the number of active Rh sites increases with increasing Rh coverage and approaches the number of sites present on one side of our Rh(111) sample (1.2×10^{15} sites). (Note: Rh particles are deposited on only one side of the SiO_2/Mo(112) sample.)

(O_2/CO) Gas Mixture Dependent Reactivity Measurements. Reactivity measurements were conducted using various gas mixture compositions (O_2/CO) to investigate the (O_2/CO) dependencies of the CO_2 oxidation reaction on the Rh/SiO_2 catalyst surfaces. Shown in Figure 2 are reactivity measurements (TOF vs 1000/T (K)) obtained on Rh/SiO_2/Mo(112) samples (with a constant Rh coverage of $\theta_{Rh} = 0.25$ ML) and comparable Rh(111) single crystals for various gas mixtures (1/1, 1/2, 1/5, and 1/10 O_2/CO). Particle data are normalized to the number of sites calculated from the data of Figure 1 for a $\theta_{Rh} = 0.25$ ML equivalent sample ($N = 8.5 \times 10^{13}$ active Rh sites). As Figure 2 illustrates, the data exhibit similar (O_2/CO) dependencies (positive order in O_2, negative order in CO) as seen on the Rh single-crystal data and previous[1−6,37] technical catalyst studies, as evidenced by the increase in reaction rate as a function of increased O_2 partial pressure. Likewise, Rh(111) single-crystal data obtained at (1/1) O_2/CO exhibit TOF values consistent with previous studies.[37] Of the four gas mixtures employed in Figure 2, the Rh particle data for the (1/1) O_2/CO mixture (though still exhibiting fair agreement) showed a slight deviation from the Rh(111) single-crystal data. TOF values over the Rh/SiO_2 surface under these reaction conditions showed TOF slightly lower than those that would be expected for the

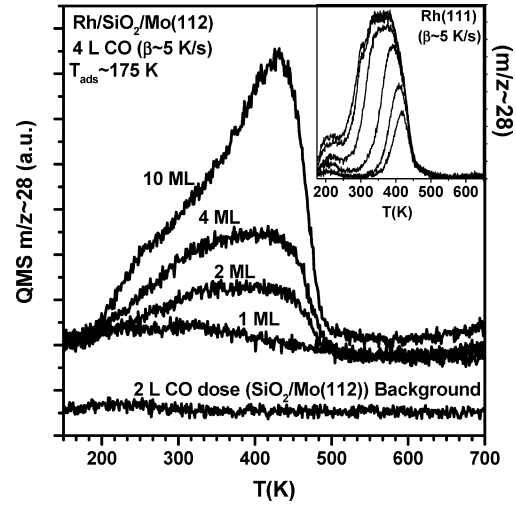

Figure 3. CO TPD from Rh/SiO_2/Mo(112) particles ($\theta_{Rh} = 1.0$, 2.0, 4.0, and 10 ML). Inset: coverage-dependent (0.25, 0.5, 1, 2, 4, and 6 langmuir CO doses) CO TPD from Rh(111).

normalization, suggesting the number of Rh active sites is less than that calculated in Figure 1a for the (1/10) O_2/CO gas mixture. Reactions run under (1/1) O_2/CO mixtures at temperatures above $T = 600$ K began to show deactivation (evidenced by lower CO_2 formation rate), which is consistent with oxidation-induced changes in the particles (to be discussed shortly).

CO TPD from Rh/SiO_2/Mo(112). Displayed in Figure 3 are results from CO TPD measurements from the Rh/SiO_2/Mo(112) samples and a Rh(111) single crystal. As discussed in the Experimental Section, Rh/SiO_2 samples of a variety of coverages ($\theta_{Rh} = 1-10$ ML) were prepared in the UHV chamber, and 4 langmuirs of CO ($P_{CO} \sim 5 \times 10^{-7}$ Torr) is dosed at $T_{ads} = 175$ K, followed by heating to $T = 700$ K at $\beta \sim 5$ K/s. TPD spectra of coverages below <0.5 ML produced TPD spectra with low QMS signals obscured by background. Also shown in the inset of Figure 3 are the TPD spectra obtained from the Rh(111) single crystal for various CO doses (0.25−6 langmuirs of CO). A saturation dose is apparent between 2−4 langmuirs of CO. CO TPD from the Rh/SiO_2 and Rh(111) sample exhibited desorption characteristics generally similar to those observed in previous studies on Rh(111) and Rh particle studies.[14,20,31] A small feature on the Rh(111) sample ($T \sim 150-200$ K) for large CO doses is believed to be due to contributions from the sample leads. We conservatively estimate that this contributes to a ±20% error in the integrated area estimates for the Rh(111) integrated area for a 4 langmuir CO dose. As will be discussed, the CO was observed to adsorb and desorb molecularly, with no indication of substantial CO dissociation. The CO TPD spectra obtained from the particles were then used to estimate the number of Rh sites on the Rh/SiO_2 samples as a function of Rh coverage, as described in the Experimental Section. Shown in Figure 4a are the values obtained from this exercise, in terms of Rh sites/cm^2, as a function of Rh coverage. As the data demonstrate, estimates of Rh sites from the TPD data increase with increasing Rh coverage, approaching the Rh site coverage for the Rh(111) single-crystal sample (1.6×10^{15} sites/cm^2). Error bars represent the estimated error (±20%) from Rh(111) TPD integration discussed above.

Rh/SiO_2 STM Results. STM images were collected on Rh/SiO_2 samples in a separate STM/UHV system. An ultrathin SiO_2 film (1 ML of SiO_2, 3 Å)[9] was grown on a Mo(112) substrate, allowing for sufficient conductivity for STM imaging. Rh metal was vapor deposited on the sample at $T = 300$ K and images

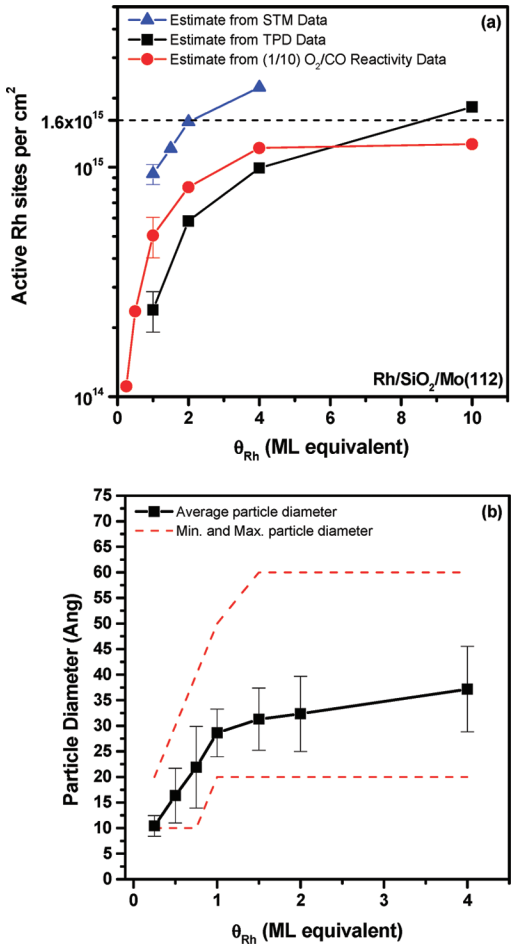

Figure 4. Number of active Rh sites/cm^2 vs Rh coverage (ML equivalent) as estimated from TPD spectra (□), (1/10) O_2/CO reactivity data (●), and STM data (▲); see text. Characteristic error bars for the data sets, shown for reference, are discussed in the text. Estimates of error in θ_{Rh} from stated coverage are ±15%; see text. Average particle diameter (in angstroms, Å) (□) and standard deviation (error bars, $\pm\sigma$) as determined from histogram data obtained from STM images. Shown by dotted lines (-----) are the minimum and maximum Rh particle diameters observed for a given Rh coverage.

taken under UHV conditions at various Rh coverages (θ_{Rh} = 0.1−4.0 ML). Shown in Figure 5a−d are four representative STM images (coverages of θ_{Rh} = 1.0, 1.5, 2.0, and 4.0 ML, respectively) from these studies. Rh particles appear as bright spots in the images, with mean Rh particle size increasing as a function of Rh coverage. Particle site densities calculated from the images show that, as the Rh coverage is increased, the particle density increases slightly from 5 × 10^{12} particles/cm^2 to 3 × 10^{13} particles/cm^2. At or below 0.5 ML Rh coverage, small Rh particles partially wet the silica surface and form quasi-2D particles scattering across the surface. A majority of Rh particles have a thickness of approximately one to two layers. The apparent size of these quasi-2D Rh particles is influenced by the variation of sample bias during imaging and increases with the increase of sample bias at above +1.0 V. As the surface Rh coverage increases, Rh particles become 3D and exhibit a hemispherical shape. The apparent size of 3D Rh particles is not influenced by the sample bias, suggesting STM measures the topographic height of 3D Rh particles.

The statistics on the particle height and diameter were then measured from these STM images of 100 nm × 100 nm in size. To remove the influence of the tip apex in size measurement, we calibrated the measured particle diameter on the basis of the Rh deposition rate. Assuming (1) the sticking probability of Rh on the thin silica film is 1 and (2) all Rh particles were exaggerated by the same factor, χ, due to the tip apex, we normalized the total calculated volume of Rh particles to the total deposition volume of Rh by solving the equation $\sum_{i=1}^{n}\{h\pi_i[3(r_i\chi)^2 + h_i^2]\}/6 = V_{dep}$. The volume equation of a spherical cap, $h\pi(3r^2 + h^2)/6$, is used here to calculate the volume of each Rh particle. V_{dep} is the amount of deposited Rh calculated from the flux rate of Rh times the deposition time. The flux rate of Rh is 0.045 ML/min, calibrated by AES breakpoint analysis on the clean Mo(112) surface. Rh AES breakpoint analysis in the STM chamber showed results similar to breakpoint analysis in the reactivity chamber (breakpoint at an AES ratio of Rh/Mo ∼ 0.5). The assumption (1) on the sticking probability of Rh should be valid, at least for high Rh coverages. The height over the calibrated particle diameter gives a ratio of about 0.4, consistent for particles of all sizes and suggests Rh particles formed a pseudohemispherical shape at the silica film surface.

On the basis of the calibrated particle height and diameter, a geometric estimate of the total surface sites of the UHV prepared sample (prereaction) can be calculated based on the equation for the spherical cap surface, $A = 2r\pi h$, for the Rh coverages in Figure 5, assuming a surface atom density of 1.6 × 10^{15} atoms/cm^2 (Rh(111) surface atom density). This assumption will likely provide an overestimate of the number of active Rh sites; especially as particles approach smaller sizes and rougher surfaces. The result of this calculation is shown in Figure 4a (▲ symbol). Also displayed in Figure 4b are the mean particle diameter (in Å, □ symbol) and standard deviation (error bars) calculated from the histogram data obtained from the θ_{Rh} = 0.1−4 ML images, along with the minimum and maximum particles sizes observed for each coverage (---- dotted lines). As the data illustrate, the mean diameter of the particles as measured by STM increases from d_p = 10 Å at 0.1 ML Rh to d_p = 35 Å for 4 ML Rh coverages, with an increasing spread in particle size as Rh coverage increases. It should be reiterated that STM images were taken on ultrathin (1 ML, 3 Å) SiO_2 films to achieve sufficient conductivity for imaging, whereas CO TPD and reactivity measurements were obtained on thicker (5 ML, 15 Å) SiO_2 films. Although it is unclear whether there exists substantial differences in the nucleation and growth or behavior of Rh particles with respect to SiO_2 film thickness, these data provide the best means at present to image particle sizes on similarly grown samples and will be used in our discussion.

Discussion

As mentioned earlier, previous kinetic studies of CO oxidation on Pt-group metal single-crystal surfaces, under similar reaction conditions, have produced numerous insights into this reaction system. These investigations have demonstrated that, under elevated-pressure conditions (pressures approaching 1 atm and CO-rich reaction conditions) and relevant catalytic temperatures (T = 450−625 K), the CO oxidation reaction on Rh (and Pd, Pt) exhibits structure-insensitive behavior; that is, observed catalytic activity does not depend upon the underlying crystal structure.[1−3] This view has been further validated by the good agreement of single-crystal data with high surface area supported catalyst data.[1−5] Technical catalyst studies employing different size Rh particles in the CO-inhibited regime, have also verified this structure-insensitive behavior (<10−676 Å particles).[6] Under such conditions, CO_2 formation is rate-limited by the CO desorption step as CO blocks sites for O_2 adsorption and

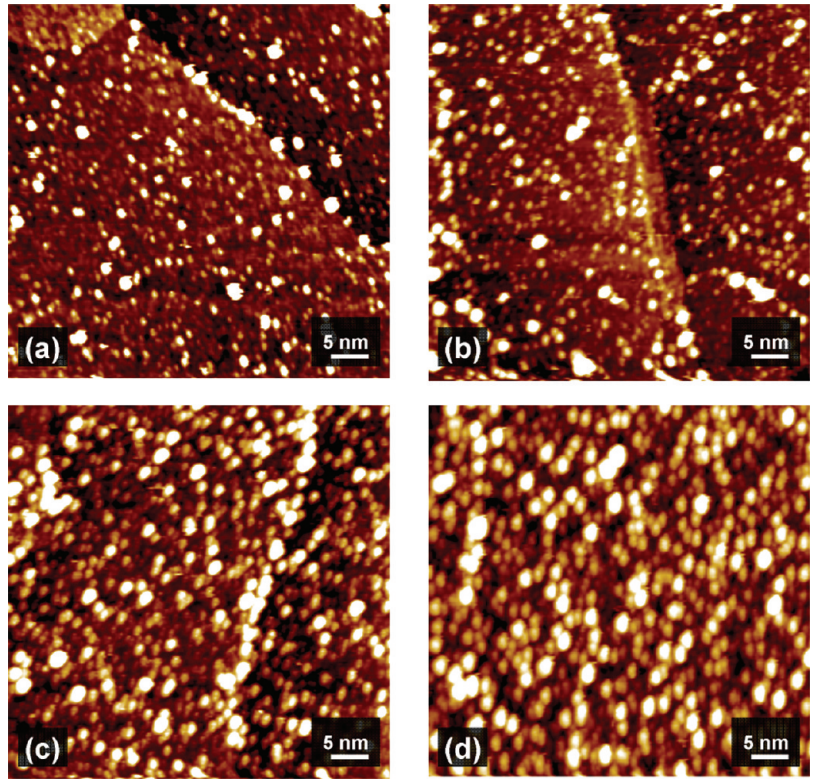

Figure 5. STM images for various coverages of Rh on Rh/(1 ML SiO_2)/Mo(112) films: (a) 1.0 ML Rh, (b) 1.5 ML Rh, (c) 2.0 ML Rh, (d) 4.0 ML Rh. Each panel is a 50 nm × 50 nm image.

dissociation. This view agrees with the observed positive order dependence on O_2 pressure, negative order dependence on CO pressure, and the similarity of the observed reaction activation energy with the CO desorption activation energy. Additionally, this is similar to the observed activation energies for CO oxidation on Pd and Pt under similar reaction conditions,[37−39] owing to the similar binding energy of CO on these metal surfaces.[32]

When oxygen begins to become a dominant surface species on the Rh and Pd surfaces (under sufficiently high temperatures and/or high oxygen partial pressures), kinetic behavior begins to deviate from this CO-dominant regime as oxygen inhibition begins to decrease the observed CO_2 formation rate.[1,2,33] Likewise, reaction measurements obtained under ultra-high-vacuum conditions (via molecular beam techniques) have shown that Rh single-crystal[58,61] and Rh/Al_2O_3 surfaces[18] can exhibit structure-sensitive reaction behavior outside of the CO-inhibited regime (i.e., surfaces containing low CO coverages).[58,61,18] Under oxygen-rich (high O_2/CO ratio) reaction conditions at elevated pressures, oxygen surface phases (such as surface or bulk oxide phases) can exist and can provide a source of surface oxygen for reaction with CO;[34] however, recent studies regarding the exact nature of the reactivity of Pt-group oxide phases have been the subject of much debate.[35−39] Whereas low-pressure studies[32,40−43] and recent high-pressure studies[30,37−39] of CO oxidation on Pt-group single crystals (Pt, Rh, Pd) have suggested that the most active phase for CO oxidation at low and high pressures is a CO-uninhibited metal surface, alternative proposals have suggested that surface oxide phases may play the key role in high reactivity on Pt-group metals under oxygen-rich conditions.[35,36,55,60] In this study, we remain focused on the CO-rich regime (low O_2/CO ratios), in which elevated-pressure reactivity behavior is known to behave as a structure-insensitive reaction limited by the CO desorption rate, with reaction kinetics reflecting traditional Langmuir−Hinshelwood behavior.[1−3,37−39] Under such conditions, CO oxidation reaction can be employed as a characterization tool to estimate the number of active Rh sites as a function of metal coverage.

First, we begin with examination of the data of Figure 1, which demonstrate similar findings and behaviors as have been observed under CO-rich reaction conditions on Rh single-crystal surfaces. Apparent reaction activation energies obtained for the $\theta_{Rh} = 0.25-10$ ML particle data all exhibited values between $E = 100-110$ kJ/mol, under the CO-rich (1/10) conditions employed. This observation strongly suggests that, similar to Rh(111) surfaces, under the conditions (P, T, O_2/CO ratios) of Figure 1, the reaction rate is limited by CO desorption (∼CO binding energy). This is a key point that we believe indicates that, under the (1/10) O_2/CO gas mixture conditions, the active portion of the Rh particle surface is primarily dominated by CO species such that CO desorption remains the rate-limiting step for reaction. The second key observation is that reaction measurements taken under the reaction conditions show reversible behavior within measurement error. In other words, reactions can be run a number of times throughout the linear reactivity range, with repeated measurements producing similar TOF values within expected error. This suggests that, whatever oxidation and/or sintering is occurring after exposure to high-pressure reaction conditions (after exposure to O_2/CO gas mixture and heating to reaction temperature), do not appear to substantially affect the reaction rate (CO_2 molecules produced/s).

Data presented in Figure 2 also illustrate similar trends to those observed on Rh single-crystal surfaces. First, reaction kinetics appear to exhibit O_2/CO dependencies similar to those observed on Rh surfaces; that is, positive order dependencies in O_2 partial pressures and negative orders in CO partial pressures. Figure 2 nicely illustrates this trend with reaction rates increasing as a function of increasing O_2/CO gas mixture ratio. Second, activation energies for the 1/10 through the 1/1 O_2/CO gas mixtures exhibit similar reaction activation energies between

$E = 100-110$ kJ/mol, suggesting that, under these conditions, the reaction rate is still primarily dictated by the rate-limiting step of CO desorption under these particular elevated-pressure conditions. Furthermore, when normalizing data for the 1/10 to 1/2 gas mixtures by the number of Rh sites obtained from Figure 1, TOF data agree very well with data obtained on the Rh(111) single crystal. Data for (1/1) O_2/CO reactivity measurements, although still lining up fairly well with single-crystal data, are slightly lower than expected when normalized by the number of sites calculated from (1/10) O_2/CO data. This is consistent with (a) a reduction in the number of active Rh sites available for reaction or (b) a decreased activity in the active site(s) on the Rh particle.

First, sintering due to thermal/pressure treatment could involve the reduction of number of active sites at higher O_2/CO ratios and temperatures. Several studies on model surfaces have demonstrated that Rh particles can exhibit agglomeration, dispersion, and morphology/shape effects on a variety of supports [theoretical,[56] (MgO),[57] (TiO_2),[23-26] (Al_2O_3)[44]] as a result of gas ambients (CO, O_2) and/or thermal treatments. For the specific case of Rh/SiO_2, ISS/XPS experiments by Kohl et al. have demonstrated thermally induced agglomeration of Rh particles deposited on Rh/SiO_2/Mo films under UHV conditions.[22] Additional work by Knözinger and co-workers[21] has also shown similar behavior for the Rh/SiO_2 surface. Particle sintering of Rh/SiO_2 samples, at high temperatures and O_2/CO ratios, could be a contributor to the slightly lower reaction rates observed for the (1/1) O_2/CO measurements of Figure 2.

A second possibility could be the increased oxidation of Rh particles, especially if particles or particle surface(s) are completely oxidized to bulk Rh oxide (Rh_2O_3). Although current debate surrounds the nature of reactivity of Pt-group metal surface oxides[55,35,36,60] compared to chemisorbed oxygen phases, it is generally accepted and observed that *bulk* oxides of Rh are less reactive than chemisorbed oxygen surfaces for CO oxidation reactions.[55,37] Bulk oxidation of small Rh particles or rough particle surfaces could result in lower reaction rates for $O_2/CO \geq 1$ mixtures. It has been shown in previous studies that, in O_2 and O_2/CO environments, Rh particles can undergo changes in oxidation state and morphology. Electron microscopy and diffraction studies by Rupprechter et al.[13] of alumina-supported Rh particles have shown that, although little change in particle morphology occurs upon annealing in vacuum to $T = 725$ K, annealing particles in 1 bar O_2 at $T = 575$ K showed thin oxide formation on the particle surfaces; heating to $T = 675-725$ K resulted in an increased thickness of oxide surrounding the metallic particle core. Reduction of oxidized particles (1 bar H_2) at low temperature $T = 525$ K produced polycrystalline particles and Rh/Rh_2O_3 layer particle surfaces; increasing reduction treatment to $T = 725$ K resulted in more fully reduced particles. Dudin et al. examined changes in particle morphology and oxidation states of Rh/MgO systems (Rh particles and films) upon exposure to O atom plasma ($P \sim 10^{-6}$ mbar; $T = 450-500$ K) and hydrogen reduction ($P \sim 5 \times 10^{-6}$ mbar; $T \sim 490$ K). Rh particles were found to be rather heterogeneous with respect to oxidation state (even within the same particle), indicating that the nature of an oxidized catalyst surface can be quite heterogeneous, despite identical oxidation conditions.[27] Oxidation and reduction treatments can also alter the surface morphology of Rh single-crystal and technical catalyst surfaces.[45,46] EXAFS studies of bulk Rh/Al_2O_3 catalysts during elevated-pressure CO oxidation reactions by Newton et al. have shown that Rh particles can rapidly oxidize at room temperature upon exposure to O_2. However, during reaction conditions, the O_2/CO gas feed ratio plays an important role in the oxidative state of the particles. For ratios of $O_2/CO < 1$ and $T > 450$ K, particles are largely metallic; under oxygen-rich conditions, an oxide Rh phase dominates the catalyst surface. Under both reducing and oxidizing conditions, 100% conversion of the O_2/CO gas feed can still be achieved, indicating both surfaces can be active for CO oxidation.[7]

Studies on supported Pd systems offer additional data for comparison. Penner et al.[47] have demonstrated oxidation of Pd particles on $Al_2O_3(0001)$ to PdO (small particles) and a thin PdO film (on large particles) under high (25 Torr) O_2 pressures and moderate temperatures ($T \sim 400$ K). Experiments conducted by Hayek and co-workers[48,49] demonstrate, using SAED and HR-TEM, that, under $P = 1$ bar O_2 and $T = 673$ K conditions, Pd/SiO_2 particles disperse and form a PdO phase, with PdO growth occurring on top of Pd particles.[48] Reduction in pure CO ($P \sim 10$ mbar at $T = 525$ K) was required to achieve reduced particles. Recent studies of well-defined Pd particles (created by organometallic decomposition) supported on MgO powders have allowed for FTIR investigations under ambient O_2/CO reaction conditions near 150 °C.[50] These results indicated that, under CO-rich gas mixtures ($O_2/CO < 2$), adsorbed CO can be observed on Pd particles via FTIR, indicating a CO-rich surface; under oxygen-rich mixtures ($O_2/CO > 2$), CO IR features are not observed, indicating a CO-deficient surface.

It has been shown on single-crystal Rh samples that bulk oxide formation on Rh can result in lower CO oxidation rates; therefore, it follows that significantly lower reaction rates should be observed on Rh particles that have been fully oxidized under sufficiently high temperatures and/or O_2/CO ratios. To further investigate this effect, additional experiments were run at higher temperatures using an oxygen-rich (1/1) O_2/CO mixture in an attempt to probe reaction conditions that result in further oxidation of Rh particles. Shown in Figure 6a,b are a series of measurements conducted on 0.25 ML Rh/SiO_2/Mo(112) samples. In panel a, Rh reactivity measurements show repeatable behavior over the linear range, with repeated TOF values within measurement error. As the reaction temperature is increased to $T = 600$ K, the reaction rate begins to roll over and subsequent reactions (denoted by numeric order) at high temperatures begin to exhibit decreasing reaction rates. To further investigate this effect, an identical sample (0.25 ML Rh/SiO_2/Mo(112)) was prepared and reactions run in a similar fashion, as shown in panel b. Reactions were repeatable over the linear CO-inhibited range, as shown in panel a. A reaction (1) was then immediately run at high temperature ($T = 650$ K), followed by a reaction (2) at $T = 525$ K. As the data illustrate, the reactivity of the sample has decreased. Furthermore, the reactivity of this experiment at $T = 650$ K is higher than the $T = 650$ K measurements of Figure 6a; this is consistent with deactivation due to reaction conditions at these higher temperatures. The Figure 6b sample is then heated in $P = 8.0$ Torr pure CO (red arrow) at $T = 525$ K, and a reaction (3) is run again on the sample at $T = 525$ K; as the results show, ~80−90% of the reactivity was reclaimed due to the CO reduction treatment. These results indicate that the Rh particles undergo deactivation at sufficiently high temperatures and oxidizing conditions. The reclamation of catalytic activity, upon reduction in pure CO, suggests that a substantial portion of deactivation is due, in part, to particle oxidation. For the case of $\theta_{Rh} = 0.25$ ML Rh particles, this point appears to occur at $T > 600$ K for (1/1) O_2/CO mixtures; deactivation conditions could be expected to differ for different Rh coverages. These observations are qualitatively consistent with previous oxidation (under oxygen-rich, moderate/high-temperature environments) and

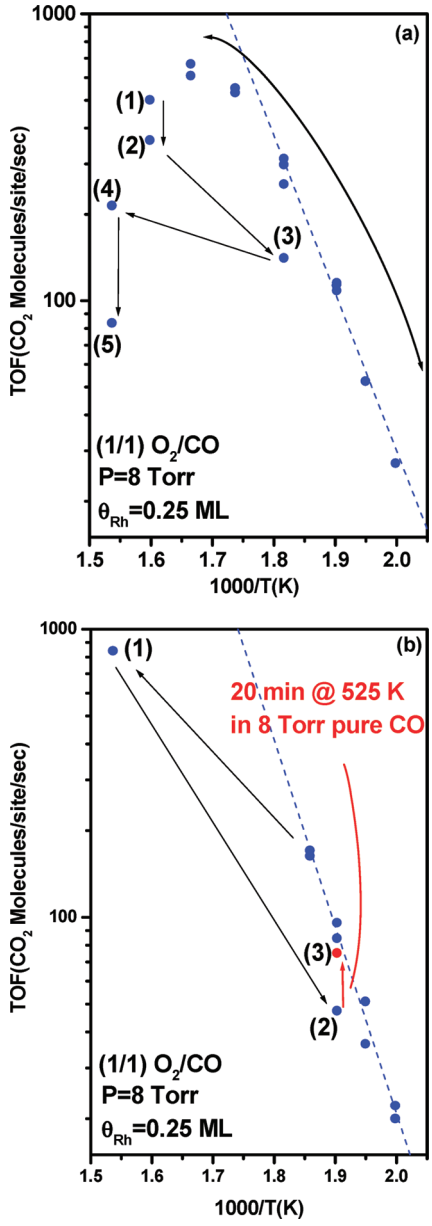

Figure 6. (a). High-temperature reactions run over $\theta_{Rh} = 0.25$ ML $Rh/SiO_2/Mo(112)$ sample with (1/1) O_2/CO. Deactivation at higher temperatures was run in sequential order (1−5). TOF normalized to the number of Rh sites obtained from 1/10 O_2/CO experiments over $\theta_{Rh} = 0.25$ ML. (b). $\theta_{Rh} = 0.25$ ML $Rh/SiO_2/Mo(112)$ sample run with (1/1) O_2/CO mixtures. Deactivation at higher temperatures was run in sequential order (1−3). Between 2 and 3, a 20 min reduction in $P = 8.0$ Torr pure CO at $T = 525$ K is conducted. TOF was normalized to the number of Rh sites obtained from (1/10) O_2/CO experiments over $\theta_{Rh} = 0.25$ ML.

reduction (under CO/H_2-reducing environments) observed on Pd[47−49] and Rh particle samples,[13,27] discussed earlier.

Under steady-state pressure and temperature conditions that produce CO-rich surfaces (such as the (1/10) O_2/CO reaction conditions employed in most of our measurements), substantial deactivation of the particles due to oxidation appears to be minimal or not detectable. Once the surface CO coverage decreases at higher temperatures, particle oxidation can occur more easily under reaction conditions. Whether the deactivation of Rh particles shown in Figure 6 is due to surface or bulk oxidation (or a mixture) of the Rh particles cannot be conclusively ascertained from these data. It is plausible that such a high-temperature treatment could have resulted in complete (bulk) oxidation of the Rh particles. Work on Pt-group metals currently underway may shed further light on this oxidation deactivation. Pt and Pd particles, metals more resistant to bulk oxidation, may exhibit oxidation-induced deactivation at higher temperatures and/or O_2 pressure conditions.

In addition to the reactivity data of Figure 1, CO TPD measurements were collected in order to provide an additional measure of the number of active sites present on the Rh particle samples. Shown in Figure 4a is a plot of the number of Rh active sites/cm^2 as calculated from the TPD measurements, STM, and reactivity data. As the data of Figure 4a illustrate, Rh site measurements from both CO-TPD and reactivity measurement techniques show fairly good agreement, with both approaching the value for the Rh(111) surface (1.6×10^{15} atoms/cm^2), as one would expect. Estimates across the coverage ranges studied by both methods agree quite well, within a factor of 2 over the Rh coverage range.

As stated earlier, CO adsorption and desorption were observed to be molecular in nature from the Rh/SiO_2 surfaces, with no evidence for substantial CO dissociation. Whereas CO dissociation is not believed to occur appreciably on low-index Rh single-crystal surfaces, it has been shown that high-index Rh single crystals (e.g., Rh(210))[51] and certain oxide-supported[15−17,19,52] Rh particles can induce dissociation of CO on the Rh surface. Freund and co-workers have demonstrated that, on ultrathin alumina substrates, Rh particles can dissociate adsorbed CO upon heating, with an activity for CO dissociation exhibiting a particle size dependence (maximum CO dissociation for particles $\sim 10^3$ atoms).[16,17] Matolin[15,19] has also demonstrated via TPD/SIMS experiments that CO can dissociate on MgO- and alumina-supported Rh particles during exposure to CO and during CO/O_2 reaction under low-pressure conditions ($\sim 10^{-6}$ Pa). Work on technical catalyst surfaces[52] under reaction conditions has shown evidence (via IR spectroscopy) for CO dissociation on alumina- and titania-supported Rh, but no evidence for appreciable CO dissociation on silica-supported Rh, indicating possible effects from support and/or particle size distribution on the different oxides. CO TPD spectra in our studies did not exhibit the high-temperature ($T \sim 520$ K) C + O recombinative desorption feature, which has been observed from TPD studies on Rh/Al_2O_3 films[59] Likewise, CO TPD experiments could be run sequentially (without sample O_2 cleaning) without a significant decrease in CO uptake that would be expected for substantial CO dissociation. Observations during reactivity measurements also did not indicate substantial CO dissociation, with respect to kinetic measurements. Indeed, during our study, we have generated Rh/SiO_2 samples and run them through long sequential series of reaction experiments in O_2/CO reaction mixtures (e.g.; 10+ reactions) without cleaning of the Rh/SiO_2 samples. No substantial decrease in activity is observed (within measurement error), which would be expected with substantial C buildup from CO dissociation. However, it should be mentioned that reactivity measurements will likely be a rather insensitive technique to investigate CO dissociation on small Rh particles under reaction conditions as it has been previously shown[15,19] that adsorbed C will be reacted away readily by oxygen even under low-pressure reaction conditions. Thus, if any CO dissociation is occurring on our Rh/SiO_2 particles, it appears that it is a small amount that does not affect the CO uptake TPD spectra or reaction kinetics (due to rapid reaction of C under reaction conditions) to an extent we can measure under our experimental conditions and measurement

sensitivities. Thus, CO uptake measurements are a reasonable technique to quantify the number of Rh active sites on Rh/SiO_2 samples.

STM measurements were conducted to provide an estimate of particle size and shape and to provide an additional method to estimate the number of active particle sites/cm^2, based on a geometric estimate. As the STM data suggests, this method appears to predict a higher number of sites than the reaction measurements. This could be due to particle morphology changes (agglomeration or sintering) that could occur upon exposure to reactive gas mixture and heating of the Rh/SiO_2 sample, as has been observed in other Rh model catalyst studies discussed previously, as the STM images are taken immediately after Rh deposition at $T = 300$ K. It could also be due to the fact that the assumption of (111) single-crystal facets may overestimate the Rh sites/cm^2 present on (110) and (100) facets present on the particle surface. This may be especially true for smaller particles. Despite these differences, it is surprising to observe that site estimates derived from all three methods fall roughly within a factor of ~3 of one another and track well with increasing Rh coverage.

It is clear from the data of Figure 4 that better agreement is achieved between the site estimates from reactivity and TPD measurements. This could be due to the fact that CO TPD and CO reactivity measurements provide a more direct measure of CO adsorption sites on the Rh particles, whereas the STM estimates arise from a geometric argument containing several simplifying assumptions. One could also speculate that this agreement results from the similar temperature treatments on the TPD (heating to $T = 700$ K) and reactivity measurements (heating to $T = 600$ K). However, the differing environments of these two methods (reactivity measurements, $P = 8.0$ Torr; TPD measurements, $P = 10^{-7}-10^{-6}$ Torr) make conclusive statements on this difficult at present, in light of the dispersion/agglomeration behavior observed in previous Rh particle studies discussed earlier.

Taken together, we interpret these results to indicate that careful reactivity experiments conducted under rich CO gas mixtures can provide a reasonable method to measure Rh active sites for CO oxidation from TOF values. This indicates that the method of Figure 1 can be used to characterize Rh/SiO_2 samples for use in surface-sensitive reactions (e.g., NO + CO), reactions whose selectivity and activity are a function of particle size and morphology. Ongoing work in our laboratory is aimed at investigating such surface-sensitive reactions and how reactivity and selectivity of such reactions at elevated-pressure conditions relate to metal coverage and particle size.

Conclusions

In summary, we have conducted an initial study of CO oxidation activity on $Rh/SiO_2/Mo(112)$ catalyst surfaces prepared and studied in situ under relevant temperature and elevated-pressure conditions. Reactivity was studied primarily under CO-rich reaction mixtures to investigate reaction kinetics. Our primary conclusions, under the experimental conditions investigated, are as follows:

(1) Results demonstrate that CO oxidation reaction on $Rh/SiO_2/Mo(112)$ model catalyst samples exhibits similar O_2/CO dependencies (negative in CO, positive in O_2), activation energies, and TOF values as observed in previous studies on Rh surfaces, under reaction conditions used. To the best of our knowledge, this is the first attempt to directly compare elevated-pressure CO oxidation reaction kinetics on Rh model catalyst surfaces to Rh single-crystal surfaces (prepared entirely in situ in UHV) under identical reaction and reactor conditions. The tandem use of model catalyst surfaces and well-defined single-crystal surfaces under identical reaction conditions can provide useful insights into the behavior of model catalyst surfaces.

(2) Estimates of Rh active sites based on reaction rates under CO-dominant conditions (1/10) O_2/CO are in good agreement with estimates obtained from TPD measurements. STM images obtained for Rh particles deposited on ultrathin SiO_2 film at $T = 300$ K provide estimates in active sites within a factor of ~3 of reactivity and TPD measurements. The good agreement of the TPD and reactivity measurements and the broad agreement of all three methods indicate that CO oxidation measurements, run under CO-rich conditions, can provide a reasonable estimate of the number of active sites present on a Rh model catalyst sample. Such characterization will be useful for future studies of particle- and structure-dependent reactions on model catalyst surfaces.

(3) Sample deactivation, consistent with oxidation, begins to occur at higher temperatures ($T > 600$ K) and O_2/CO ratios > 1/1 for $\theta_{Rh} = 0.25$ ML. Particle reactivity can be partially recovered by reduction in pure CO.

Acknowledgment. We gratefully acknowledge support of this work by the Department of Energy, Office of Basic Energy Sciences, Division of Chemical Sciences, Geosciences, and Biosciences (DE-FG02-95ER-14511) and the Robert A. Welch Foundation.

References and Notes

(1) Goodman, D. W.; Peden, C. H. F. *J. Phys. Chem.* **1986**, *90*, 4839.
(2) Peden, C. H. F.; Goodman, D. W.; Blair, D. S.; Berlowitz, P. J.; Fisher, G. B.; Oh, S. H. *J. Phys. Chem.* **1988**, *92*, 1563.
(3) Oh, S. H.; Fisher, G. B.; Carpenter, J. E.; Goodman, D. W. *J. Catal.* **1986**, *100*, 360.
(4) Kiss, J. T.; Gonzalez, R. D. *J. Phys. Chem.* **1984**, *88*, 898.
(5) Cant, N. W.; Hicks, P. C.; Lennon, B. S. *J. Catal.* **1978**, *54*, 372.
(6) Oh, S. H.; Eickel, C. C. *J. Catal.* **1991**, *128*, 526.
(7) Newton, M. A.; Dent, A. J.; Diaz-Moreno, S.; Fiddy, S. G.; Jyoti, B.; Evans, J. *Chem.—Eur. J.* **2006**, *12*, 1975.
(8) Henry, C. R. *Surf. Sci. Rep.* **1998**, *31*, 231.
(9) Chen, M. S.; Santra, A. K.; Goodman, D. W. *Phys. Rev. B* **2004**, *69*, 155404-1–155404-7.
(10) Schroeder, T.; Giorgi, J. B.; Bäumer, M.; Freund, H.-J. *Phys. Rev. B* **2002**, *66*, 165422-1–165422-11.
(11) Schroeder, T.; Adelt, M.; Richter, B.; Naschitzki, M.; Baumer, M.; Freund, H.-J. *Surf. Rev. Lett.* **2000**, *7*, 7.
(12) Xu, X.; Goodman, D. W. *Appl. Phys. Lett.* **1992**, *61*, 774.
(13) Rupprechter, G.; Hayek, K.; Hofmeister, H. *J. Catal.* **1998**, *173*, 409.
(14) Belton, D. N.; Schmeig, S. J. *Surf. Sci.* **1988**, *202*, 238.
(15) Matolín, V.; Mašek, K.; Elyakhloufi, M. H.; Gillet, E. *J. Catal.* **1993**, *143*, 492.
(16) Andersson, S.; Frank, M.; Sandell, A.; Giertz, A.; Brena, B.; Brühwiler, P. A.; Mårtensson, N.; Libuda, J.; Baümer, M.; Freund, H.-J. *J. Chem. Phys.* **1998**, *108*, 2967.
(17) Frank, M.; Andersson, S.; Libuda, J.; Stempel, S.; Sandell, A.; Brena, B.; Giertz, A.; Brühwiler, P. A.; Bäumer, M.; Mårtensson, N.; Freund, H.-J. *Chem. Phys. Lett.* **1997**, *279*, 92.
(18) Nehasil, V.; Stará, I.; Matolín, V. *Surf. Sci.* **1996**, *352*, 305.
(19) Matolín, V.; Elyakhloufi, M. H.; Mašek, K.; Gillet, E. *Catal. Lett.* **1993**, *21*, 175.
(20) Zhu, Y.; Schmidt, L. D. *Surf. Sci.* **1983**, *129*, 107.
(21) Labich, S.; Kohl, A.; Taglauer, E.; Knözinger, H. *J. Chem. Phys.* **1998**, *109*, 2052.
(22) Kohl, A.; Labich, S.; Taglauer, E.; Knözinger, H. *Surf. Sci.* **2000**, *454*, 974.
(23) Labich, S.; Taglauer, E.; Knözinger, H. *Top. Catal.* **2001**, *14*, 153.
(24) Berkó, A.; Solymosi, F. *J. Catal.* **1999**, *183*, 91.
(25) Óvári, L.; Kiss, J. *Appl. Surf. Sci.* **2006**, *252*, 8624.
(26) Park, J. B.; Ratliff, J. S.; Ma, S.; Chen, D. A. *J. Phys. Chem. C* **2007**, *111*, 2165.
(27) Dudin, P.; Barinov, A.; Gregoratti, L.; Scaini, D.; He, Y. B.; Over, H.; Kiskinova, M. *J. Phys. Chem. C* **2008**, *112*, 9040–9044.

(28) Zhang, Y.; Grass, M. E.; Kuhn, J. N.; Tao, F.; Habas, S. E.; Huang, W.; Yang, P.; Somorjai, G. A. *J. Am. Chem. Soc.* **2008**, *130*, 5868.
(29) Szanyi, J.; Goodman, D. W. *Rev. Sci. Instrum.* **1993**, *64*, 2350.
(30) Chen, M. S.; Cai, Y.; Yan, Z.; Gath, K. K.; Axnanda, S.; Goodman, D. W. *Surf. Sci.* **2007**, *601*, 5326.
(31) Linke, R.; Curulla, D.; Hopstaken, M. J. P.; Niemantsverdriet, J. W. *J. Chem. Phys.* **2001**, *115*, 8209.
(32) Engel, T.; Ertl, G. *Adv. Catal.* **1979**, *28*, 1.
(33) Berlowitz, P. J.; Peden, C. H. F.; Goodman, D. W. *J. Phys. Chem.* **1988**, *92*, 5213.
(34) Lundgren, E.; Gustafson, J.; Resta, A.; Weissenrieder, J.; Mikkelsen, A.; Andersen, J. N.; Köhler, L.; Kresse, G.; Klikovits, J.; Biederman, A.; Schmid, M.; Varga, P. *J. Electron Spectrosc. Relat. Phenom.* **2005**, *144*, 367.
(35) Hendriksen, B. L. M.; Frenken, J. W. M. *Phys. Rev. Lett.* **2002**, *89*, 046101−1.
(36) Hendriksen, B. L. M.; Bobaru, S. C.; Frenken, J. W. M. *Surf. Sci.* **2004**, *552*, 229.
(37) Gao, F.; Cai, Y.; Gath, K. K.; Wang, Y.; Chen, M. S.; Guo, Q. L.; Goodman, D. W. *J. Phys. Chem. C* **2009**, *113*, 182–192.
(38) Gao, F.; Wang, Y.; Cai, Y.; Goodman, D. W. *J. Phys. Chem. C* **2009**, *113*, 174–181.
(39) Gao, F.; McClure, S. M.; Cai, Y.; Gath, K. K.; Wang, Y.; Chen, M. S.; Guo, Q. L.; Goodman, D. W. *Surf. Sci.* **2009**, *603*, 65–70.
(40) Jones, I. Z.; Bennett, R. A.; Bowker, M. *Surf. Sci.* **1999**, *439*, 235.
(41) Miners, J. H.; Cerasari, S.; Efstathiou, V.; Kim, M.; Woodruff, D. P. *J. Chem. Phys.* **2002**, *117*, 885.
(42) Schwartz, S. B.; Schmidt, L. D.; Fisher, G. B. *J. Phys. Chem.* **1986**, *90*, 6194.
(43) Leung, L.-W. H.; Goodman, D. W. *Catal. Lett.* **1990**, *5*, 353.
(44) Frank, M.; Kühnemuth, R.; Bäumer, M.; Freund, H.-J. *Surf. Sci.* **1999**, *427*, 288.
(45) Logan, A. D.; Sharoudi, K.; Datye, A. K. *J. Phys. Chem.* **1991**, *95*, 5568.
(46) Kalakkad, D.; Anderson, S. L.; Logan, A. D.; Peña, J.; Braunschweig, E. J.; Peden, C. H. F.; Datye, A. K. *J. Phys. Chem.* **1993**, *97*, 1437.
(47) Penner, S.; Bera, P.; Pedersen, S.; Ngo, L. T.; Harris, J. J. W.; Campbell, C. T. *J. Phys. Chem. B* **2006**, *110*, 24577.
(48) Penner, S.; Wang, D.; Jenewein, B.; Gabasch, H.; Klötzer, B.; Knop-Gericke, A.; Schlögl, R.; Hayek, K. *J. Chem. Phys.* **2006**, *125*, 094703.
(49) Gabasch, H.; Knop-Gericke, A.; Schlögl, R.; Borasio, M.; Weilach, C.; Rupprecther, G.; Penner, S.; Jenewein, B.; Hayek, K.; Klötzer, B. *Phys. Chem. Chem. Phys.* **2007**, *9*, 533.
(50) Borchert, H.; Jürgens, B.; Zielasek, V.; Rupprechter, G.; Giorgio, S.; Henry, C. R.; Bäumer, M. *J. Catal.* **2007**, *247*, 145.
(51) Rebholz, M.; Prins, R.; Kruse, N. *Surf. Sci. Lett.* **1991**, *259*, L797.
(52) Trautmann, S.; Baerns, M. *J. Catal.* **1994**, *150*, 335.
(53) Grass, M. E.; Zhang, Y.; Butcher, D. R.; Park, J. Y.; Li, Y.; Bluhm, H.; Bratlie, K. M.; Zhang, T.; Somorjai, G. A. *Angew. Chem., Int. Ed.* **2008**, *47*, 8893.
(54) Tao, F.; Grass, M. E.; Zhang, Y.; Butcher, D. R.; Renzas, J. R.; Liu, Z.; Chung, J. Y.; Mun, B. S.; Miquel Salmeron, M.; Somorjai, G. A. *Science* **2008**, *322*, 5903.
(55) Gustafson, J.; Westerstroem, R.; Mikkelsen, A.; Torrelles, X.; Balmes, O.; Bovet, N.; Andersen, J. N.; Baddeley, C. J.; Lundgren, E. *Phys. Rev. B* **2008**, *78*, 045423.
(56) Mittendorfer, F.; Seriani, N.; Dubay, O.; Kresse, G. *Phys. Rev. B* **2007**, *76*, 233413.
(57) Nolte, P.; Stierle, A.; Jin-Phillipp, N. Y.; Kasper, N.; Schulli, T. U.; Dosch, H. *Science* **2008**, *321*, 1654.
(58) Hopstaken, M. J. P.; Niemantsverdriet, J. W. *J. Chem. Phys.* **2000**, *113*, 5457.
(59) Matolín, V.; Mašek, K.; Elyakhloufi, M. H.; Gillet, E. *J. Catal.* **1993**, *143*, 492.
(60) Carlsson, P.-A.; Zhdanov, V. P.; Skoglundh, M. *Phys. Chem. Chem. Phys.* **2006**, *8*, 2703.
(61) Bowker, M.; Guo, Q.; Li, Y.; Joyner, R. W. *Catal. Lett.* **1993**, *18*, 119.
(62) Rupprechter, G.; Weilach, C. *J. Phys.: Condens. Matter* **2008**, 184019.
(63) Rupprechter, G. *Catal. Today* **2007**, *126*, 3.
(64) Poppa, H. *Catal. Rev.* **1993**, *35*, 359.

JP808953V